(Received 19 May 2024, Accepted 11 July 2024, Scheduled 4 August 2024)

# An AMC-Backed Dual-Band Gain-Enhanced Wearable Antenna with Low SAR for WLAN/WBAN Applications

Regalla Narendra Reddy[1, *], Nalam V. Koteswara Rao[2], and Dasari Rama Krishna[1]

[1]*ECE Department, University College of Engineering, Osmania University, Hyderabad, Telengana, India*
[2]*ECE Department, Chaitanya Bharathi Institute of Technology, Hyderabad, Telangana, India*

**ABSTRACT:** The advancement of wireless communication technology demands antennas that can achieve significant gain while functioning across diverse frequency ranges. Numerous studies have aimed to enhance the gain and radiation properties of such antennas. However, when these antennas operate near the human body, their performance regarding return loss, gain, radiation pattern, and specific absorption rate (SAR) are influenced by the interaction and absorption of human tissue. To enhance overall antenna performance, artificial magnetic conductor (AMC) surfaces have been introduced. Numerous studies have been conducted to improve antenna performance through the use of AMC surfaces. This paper proposes a coplanar waveguide (CPW)-fed wearable antenna integrated with an AMC array. The integrated antenna is expected to operate at both 2.45 GHz and 5.5 GHz, making it suitable for applications in wireless local area networks (WLAN) and wireless body area networks (WBAN). The study focuses on the benefits of the integrated antenna, highlighting advantages such as improved gain and lowered SAR in comparison to the antenna alone. These improvements are validated through both simulated and measured outcomes. This antenna, featuring a simple feed structure, low cost, and ease of fabrication, is a promising option for wearable medical applications.

## 1. INTRODUCTION

In recent years, significant interest has been growing in the design of wireless body area networks (WBAN) due to numerous applications, such as military, health monitoring, and medicine [1]. The WBAN system collects and transmits necessary data to a distant location, enabling daily remote monitoring of the condition of the wearer so that decisions can be made to safeguard their life. In wearable devices, an efficient wearable antenna is crucial for maintaining a reliable communication link with the external unit [2]. Since wireless technology has advanced, many systems can now function in various frequency bands. However, the effectiveness of antennas within these systems largely determines their ability to operate across diverse frequency ranges, with each antenna covering one or multiple frequency bands. Thus, it is preferable to have a single antenna to support the different operational frequency ranges of several wireless communication systems.

In the literature, several techniques have been proposed to create a multi-band resonance of the antenna. One of the most popular approaches is to include slots within the patch radiators [3]. However, the radiation patterns of these antennas have been impacted to some extent. Furthermore, a novel concentric circular patch antenna employing shorting vias and a mu-negative transmission line (MNG-TL) has been presented in [4]. However, excessive utilization of vias raises the complexity of the design and introduces electrical losses. Another widely used approach is to gap-couple primary patch radiators to parasitic patches or strips. In [5], a T-shaped patch antenna including several parasitic patches and shorting vias has been introduced to create additional resonances. It has been noticed that the antenna does not provide a significant gain at the upper resonating frequency.

Recently, there has been a growing interest among researchers in utilizing metamaterials (MTMs) to design multi-resonance antennas [6, 7]. In [6], a dual-band zeroth-order resonating (ZOR) antenna has been proposed. The proposed metamaterial antenna has been observed to exhibit dual-band behaviour, featuring impedance bandwidths of 5% and 59.9% at the frequencies centered around 1.22 GHz and 3.97 GHz, respectively. A metamaterial structure based dual-band antenna for WLAN applications has been suggested in [7]. However, the antenna has exhibited reduced gain. To optimize the electrical length and minimize back radiation, a dual-band folded-cavity antenna incorporating lumped components has been created [8]. However, its use for wearable applications might be limited due to the inclusion of lumped elements and a multilayer design. In addition to multi-band characteristics, for an antenna to be considered in the wearable industry, it must exhibit acceptable gain and a low SAR based on its intended application.

One of the most common approaches to enhancing antenna gain is to use artificial magnetic conductors (AMCs) as a reflective backing for the wearable antenna. As a result, surface waves are significantly decreased, and the antenna exhibits an increase in its total gain and a reduction in SAR. A dual-band textile antenna in combination with an AMC plane for WLAN applications has been proposed in [9]. However, the antenna has exhibited a low gain at the desired frequencies. In [10], a

* Corresponding author: Regalla Narendra Reddy (narendra.r@uceou.edu).

**TABLE 1**. Optimized dimensions of the required antenna.

| Parameters | a | b | c | d | e | m | n | p | q | u | v | L | W | S |
|---|---|---|---|---|---|---|---|---|---|---|---|---|---|---|
| Dimensions (mm) | 18.2 | 4.7 | 5 | 5.5 | 12.2 | 13.0 | 8.5 | 12.0 | 23.9 | 1.5 | 1.5 | 26 | 35 | 5.5 |

dual-band monopole antenna incorporating an AMC structure was introduced to enhance radiation characteristics and achieve higher gain. However, the antenna has exhibited less gain. To enhance the bandwidth with the required gain, a dipole antenna with slots utilising an artificial magnetic conductor has been proposed in [11]. Although the gain in [12] is greater than 10 dB, these antennas have complex structures and occupy a considerable physical footprint, thereby limiting their utilization. As a result, designing a multi-band antenna with improved gain, low SAR, low cost, and light weight remains a challenge.

In this study, a dual-band wearable antenna is proposed to operate at 2.45 GHz and 5.5 GHz for applications in WLAN/WBAN. The antenna is integrated with a $3 \times 3$ AMC array to minimize backward radiation by enhancing its performance when being used on the human body. Furthermore, by integrating the AMC array, the specific absorption rate (SAR) is significantly reduced by over 90% compared to an isolated co-planar waveguide (CPW)-fed antenna. The fabricated CPW-antenna prototype, along with the AMC array, was tested on various human body models, demonstrating its effectiveness for WLAN/WBAN communication systems by offering multiband performance, gain enhancement, and compliance with SAR requirements.

## 2. A COMPREHENSIVE APPROACH TO ANTENNA DEVELOPMENT

### 2.1. Antenna Configuration and Geometry

Figure 1 illustrates the schematic layout of the antenna along with the essential parameters for antenna development. The antenna element is fabricated using an economical FR-4 substrate with a relative permittivity ($\varepsilon_r$) of 4.4 and a loss tangent ($\tan\delta$) of 0.02, with a substrate height ($h$) of 0.2 mm. The overall dimensions of the coplanar waveguide (CPW)-fed antenna are $26 \times 35 \times 0.2\,\text{mm}^2$. The optimised dimensions of the required antenna are presented in Table 1.

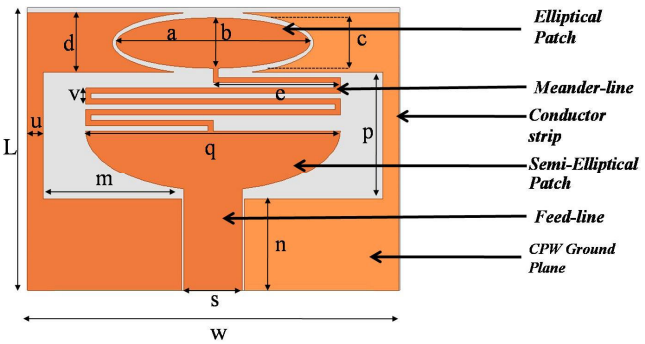


**FIGURE 1**. A schematic representation of the antenna with marked dimensions.

### 2.2. Equivalent Circuit Model Corresponding to the Proposed Antenna

Inductors, capacitors, and resistors serve as essential components in microwave circuits and antennas. Inductors can take various shapes, such as elliptical, semi-elliptical, rectangular, circular, or meandering ones, each affecting their performance. The ability of an inductor to carry current is influenced by factors like conductor width and thickness. Similarly, capacitors can be realized by introducing gaps between conductors [13]. An equivalent circuit model of the proposed structure is exhibited in Figure 2, in which series inductance $L_R$ shows the inductance associated with a signal patch composed of an elliptical patch, a meander line, a feed line, and a semi-elliptical patch, whereas series capacitance $C_L$ represents the capacitance attributed to the patches and parasitic capacitance provided by the meandered line inductor. Further, in order to create a multiband resonance, the shunt inductance ($L_L$) is realized by a conductor strip connected to CPW ground, and the shunt capacitance ($C_R$) can be realized by the gap between the signal patch and the conductor strip. In addition, the shunt capacitance ($C_g$) can be realized by the gap between the elliptical patch and the conductor strip. Furthermore, resistance $R$ and conductance $G$ describe the losses in the conductor and substrate, and for a loss-less transmission line, $R = 0$ and $G = 0$. Therefore, the equivalent circuit model of the antenna illustrated in Figure 1 represents a lossless composite right hand/left hand-transmission line (CRLH-TL) [14], as shown in Figure 2.

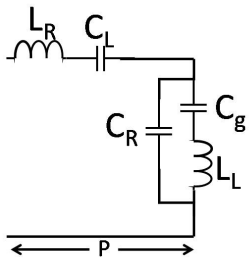


**FIGURE 2**. Approximate equivalent circuit model of the intended antenna.

Consequently, the characteristic impedance $Z_c$ and Bloch-propagation constant $\beta$ of the periodic structure are defined by

$$Z_c = \sqrt{\frac{Z'_{\text{series}}}{Y'_{\text{shunt}}}} \tag{1}$$

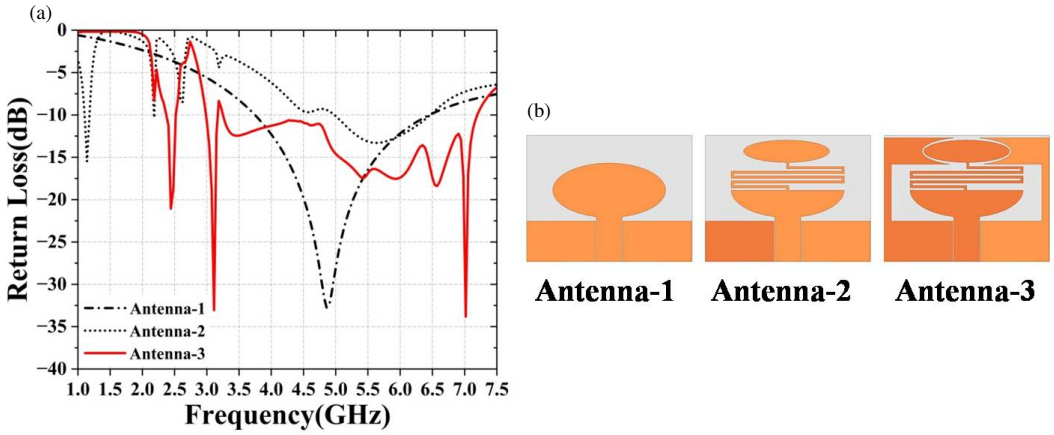


**FIGURE 3**. (a) Comparison of return loss across various stages of antenna development. (b) The schematic representation of the proposed antenna at various stages of its structural development.

where

$$Z'_{\text{series}} = j\left(\omega L_R - \frac{1}{\omega C_L}\right),$$

$$Y'_{\text{shunt}} = j\omega C_R + j\left(\omega C_g - \frac{1}{\omega L_L}\right)$$

Here the left-hand (LH)-inductive branch of the standard CRLH metamaterial [14] is transformed into the impedance $Z_{L_C+C_g} = j\omega L_L - j/(\omega C_g)$. Due to the very large value of the $C_g$ compared to the inductor, the resultant impedance $Z_{L_C+C_g} \approx L_L$.

$$\beta = \frac{1}{p}\cos^{-1}\left[1 + \frac{Z'_{\text{series}}Y'_{\text{shunt}}}{2}\right] \quad (2)$$

where '$p$' represents the physical length of the unit cell, and two resonant frequencies are associated with shunt and series resonant circuits, denoted as $\omega_{sh}$ and $\omega_{se}$, respectively. It is widely acknowledged that in an unbalanced unit cell, where $\omega_{sh}$ does not equal $\omega_{se}$, the resonant condition of CRLH is determined by the type of open or short-circuited termination and supports the relationship listed below

$$\beta_n p = \frac{n\pi p}{l} = \frac{n\pi}{N}\,(n = 0, \pm1, \pm2, \pm3..... \pm(N-1)) \quad (3)$$

Here $n$, $l$, and $N$ are the mode number, overall length of the resonator, and number of unit cells, respectively. Additionally, in the case of an open-ended lossless CRLH-TL, the input impedance can be expressed as

$$Z_{\text{in, open}} \overset{\beta\to 0}{\cong} Z_C\frac{1}{j\beta l} = \frac{1}{Y'_{\text{shunt}(Np)}} \quad (4)$$

As a result of the introduction of the capacitance $C_g$, the open-ended resonance $\omega_{sh}^{\text{open}}$ is determined by the shunt resonating tank circuit [14].

$$\omega_{sh}^{\text{open}} = \sqrt{\left(\omega_{sh}^2 + \omega_g^2\right)} \quad (5)$$

where $\omega_{sh} = \frac{1}{\sqrt{L_L C_R}}$, $\omega_g = \frac{1}{\sqrt{L_L C_g}}$ and $\omega_{se} = \frac{1}{\sqrt{L_R C_L}}$, $\omega_{sh}^{\text{open}} = \sqrt{\left(\frac{C_R+C_g}{L_L(C_R C_g)}\right)}$. Consequently, the shunt resonance's quality factor can be obtained by assuming that the electrical and magnetic energy stored in $C_g$ and $C_R(W_e)$ and $L_L(W_m)$ are equal [15]. Therefore

$$Q = \frac{2\omega_{sh}^{\text{open}} W_m}{P_{\text{loss}}} = \frac{1/G}{\omega_{sh}^{\text{open}} L_L} = \frac{1}{G}\sqrt{\left(\frac{C_R C_g}{L_L\,(C_R + C_g)}\right)} \quad (6)$$

The relationship between the impedance bandwidth of an antenna and its quality factor ($Q$) is demonstrated by Equation (6), indicating that a wider bandwidth can be achieved by either increasing the shunt inductance, reducing the shunt capacitance, or both. This adjustment results in a broader frequency range over which the antenna can efficiently operate. However, in accordance with the Chu limits [16, 17] governing electrically small antennas, there exists a limitation on the maximum achievable bandwidth, which is determined by the following relationship:

$$\text{FBW}_{\max} = \frac{s-1}{\eta\sqrt{s}}\left(\frac{1}{k^3a^3} + \frac{1}{ka}\right)^{-1} \quad (7)$$

where "$a$" denotes the sphere's radius surrounding the antenna's maximum dimension, "$k$" the wave number of the air, and "$s$" the voltage standing wave ratio (VSWR).

### 2.3. The Procedural Steps for Implementing the Desired Antenna Configuration

The structural evolution of antenna-3, or the final antenna, is displayed in Figure 3(b), and Figure 3(a) displays the equivalent return loss ($S_{11}$). A fundamental resonance mode is generated at 4.75 GHz by antenna-1, i.e., a basic symmetrical CPW-fed elliptical patch, as shown in Figure 3(b). The symmetrical patch has been transformed into an antenna inspired by metamaterials (MTMs) with a meandering line connecting the elliptical and semi-elliptical patches; this combination is referred to

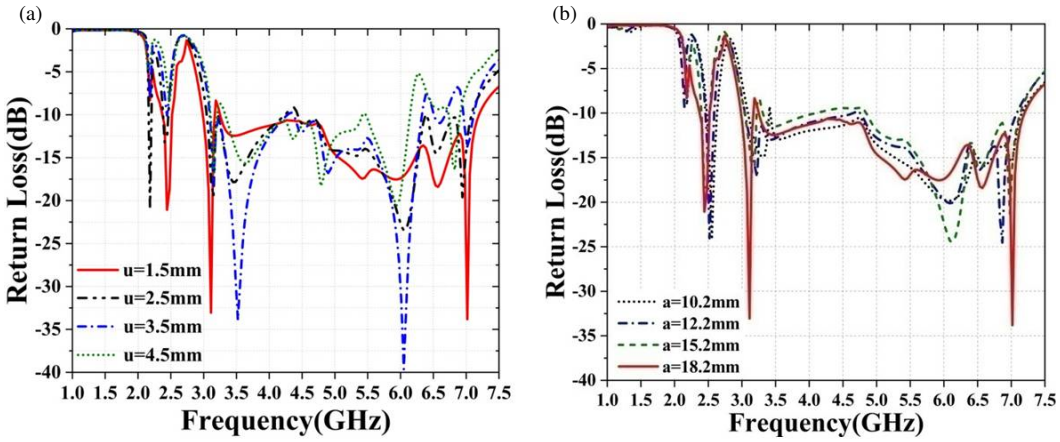


**FIGURE 4**. (a) Plot showing return loss for different widths of conductor strip '$u$' connected to CPW ground. (b) Plot showing return loss for different major axis length '$a$' of elliptical patch.

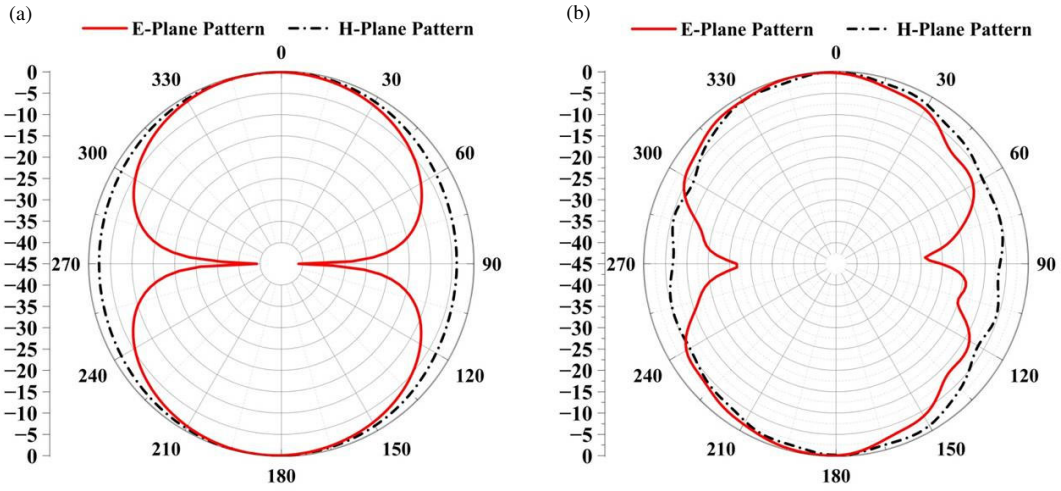


**FIGURE 5**. Radiation pattern of antenna-3 (a) at 2.45 GHz, (b) at 5.5 GHz.

as a signal patch and is presented as antenna-2 in Figure 3(b). As illustrated in Figure 3(a), this configuration exhibits multi-band operation and will result in a degradation of the antenna impedance bandwidth.

Furthermore, to get the required frequencies of 2.45 GHz and 5.5 GHz, the antenna resonances can be realized by manipulating its shunt reactance, which comprises a shunt inductance ($L_L$) realized by using a conductor strip connected to CPW ground, a capacitor ($C_g$) realized between the elliptical patch and conductor strip, and a shunt capacitance ($C_R$) between the signal patch and the conductor strip connected to CPW ground and presented as antenna-3 as shown in Figure 3(b). The resultant antenna, i.e., antenna-3, operates at 2.45 GHz and 5.5 GHz. In addition, it exhibits an impedance bandwidth of 76.92% (3.2–7.2 GHz) and 8.20% (2.3–2.5 GHz) for $S_{11} < 10$ dB, as shown in Figure 3(a). Furthermore, it also exhibits a 150 MHz bandwidth between 3 and 3.15 GHz.

Here a wider bandwidth can be achieved by increasing shunt inductance ($L_L$) and/or reducing shunt capacitance ($C_R$) of the antenna, as the impedance bandwidth is inversely proportional to $Q$, as shown by Equation (6). The shunt inductance ($L_L$) can be increased in proportion to the length of the conductor strip connected to CPW ground. Furthermore, the shunt capacitance ($C_R$) can be decreased in proportion to the increase in the gap between the conductor strip and signal patch by decreasing the width of the conductor strip '$u$' connected to the CPW ground plane. Figure 4(a) depicts a reduction in the impedance bandwidth within the range of 3.2 to 7.2 GHz as the width of the conductor strip '$u$' connected to CPW ground increases. However, the change in '$u$' does not significantly affect the lower resonance frequency of 2.45 GHz.

Further, Figure 4(b) illustrates how the lower resonance frequency increases as the major axis length '$a$' of the elliptical patch decreases. This increase occurs because reducing '$a$' widens the gap between the elliptical patch and the conductor strip, leading to a decrease in capacitance. Consequently, the lower resonant frequency increases. However, the bandwidth that is available between 3.2 and 7.2 GHz is not significantly affected by the fluctuation of '$a$'. Figures 5(a) and (b) illustrate the radiation pattern of the antenna in a normalized polar plot representation at 2.45 GHz and 5.5 GHz, respectively. It has been observed that the simulated gain at 2.45 GHz and 5.5 GHz

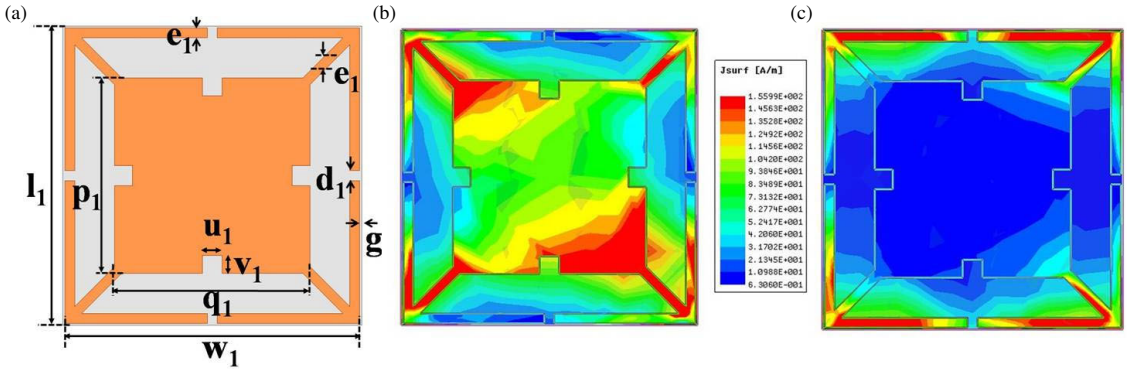


**FIGURE 6**. (a) Schematic view of the proposed AMC unit cell. (b) Surface current distribution at 2.45 GHz. (c) Surface current distribution at 5.50 GHz.

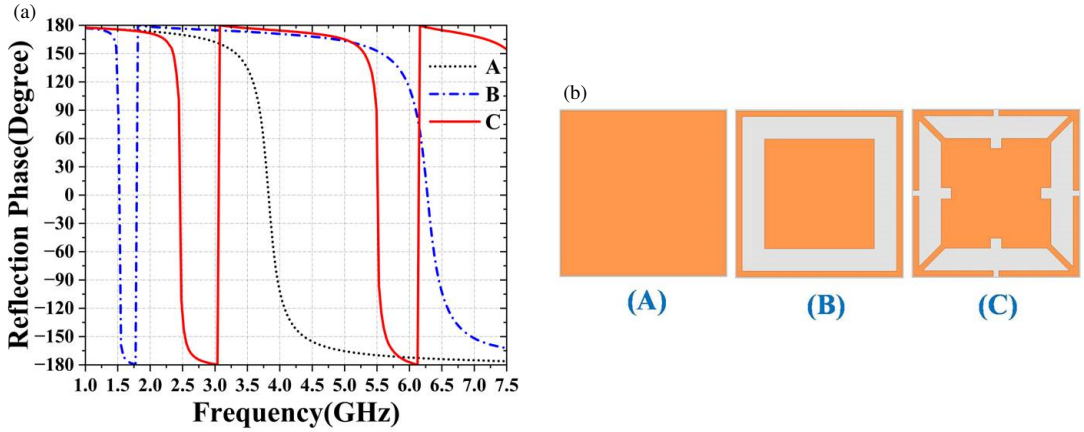


**FIGURE 7**. (a) Simulated reflection phase characteristics of the AMC unit cells A, B, C. (b) Layout of different AMC unit cells.

is −2.5 dBi and 3.5 dBi, respectively. Moreover, there is a significant front-to-back (F/B) ratio observed at both frequencies, which results in an increase in the SAR. If an antenna has to be used in wearable applications, this is undesirable. Therefore, to improve both the gain and front-to-back (F/B) ratio, integrating the antenna with an AMC array becomes necessary.

## 3. ANTENNA INTEGRATION WITH THE AMC ARRAY

### 3.1. Structural Layout of the AMC Unit Cell

The unit cell of the AMC structure is exhibited in Figure 6(a), and it is fabricated on an FR4 substrate with a thickness of 1 mm and sized at $14.8 \times 14.8\,\text{mm}^2$. The optimized parameters of the unit cell as exhibited in Figure 6(a) are detailed as follows: $l_1 = 14.8\,\text{mm}$, $w_1 = 14.8\,\text{mm}$, $p_1 = 9.8\,\text{mm}$, $q_1 = 9.8\,\text{mm}$, $u_1 = 1.0\,\text{mm}$, $v_1 = 1.0\,\text{mm}$, $e_1 = 0.5\,\text{mm}$, $d_1 = 0.5\,\text{mm}$, $g = 0.2\,\text{mm}$. The structural evolution of the unit cell is exhibited in Figure 7(b). The initial layout is based on the fundamental rectangular patch unit cell 'A', as shown in Figure 7(b). The unit cell has exhibited a reflection phase of zero degrees at 3.85 GHz. In order to enable dual-band behavior by adding additional inductance or capacitance [18], the square patch is replaced with a square patch encircled by a square ring, such as unit cell 'B'. Even though the unit cell has exhibited dual-frequency phenomena, the working frequencies of the antenna are not in sync with these frequencies, as shown in Figure 7(a). In order to get the desired frequencies, the capacitance associated with the centre square patch and the overall capacitances of the unit cell have been modified and represented as unit cell 'C'. At the lowest frequency, the whole unit cell contributes to the overall capacitance. However, at higher frequencies, distinct segments of the unit cell exert a significant influence on the capacitance of the structure [19]. Figure 7(a) illustrates the simulated reflection phase characteristics of several unit cell layouts when a plane wave is incident normally upon them. It has been noted that the reflection phase value of the necessary unit cell 'C' attains a value of 0° at 2.45 GHz and 5.5 GHz. Figures 6(b) and (c) present the distribution of surface current on the AMC unit cell at 2.45 GHz and 5.5 GHz, respectively.

It has been noticed that at 5.5 GHz, a significant current is distributed only in certain portions of the unit cell; however, at 2.45 GHz, the current is distributed around the sides of the square patch and even extends into the square slit ring. This indicates that the metamaterial effective resonant length has been increased compared to 5.5 GHz, providing further validation for the dual-band characteristics of the AMC unit cell. Moreover, the zero-phase reflection frequencies of the AMC structure align with the operating bands of the antenna, making it appropriate for integration with the dual-band CPW-fed antenna.

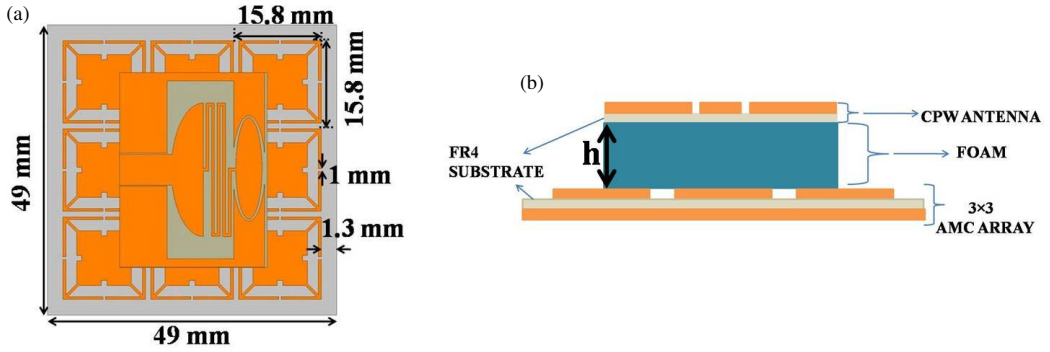


**FIGURE 8**. (a) Top view of the integrated antenna layout. (b) Side view of the integrated antenna layout.

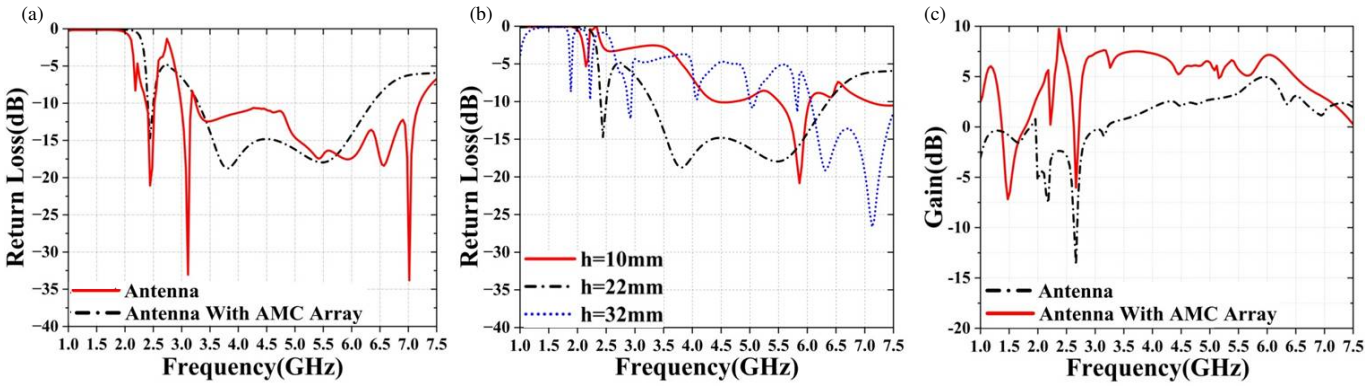


**FIGURE 9**. (a) Comparison of return loss between the antenna and the antenna with AMC array. (b) Plot showing return loss for different values of gap width '$h$' between the antenna and the antenna with AMC array. (c) Comparison of gain between the antenna and the antenna with AMC array.

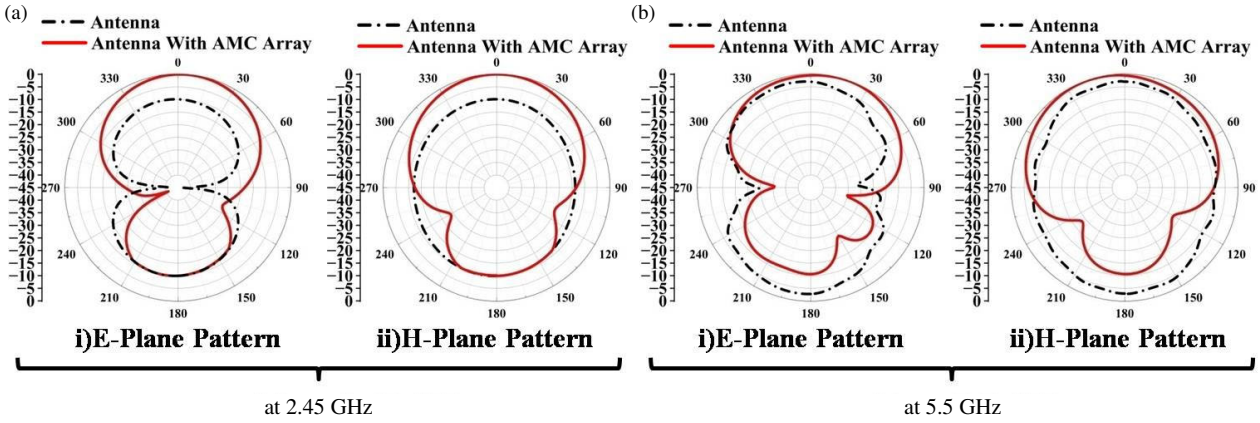


**FIGURE 10**. Radiation pattern of antenna with/without AMC array (a) at 2.45 GHz, (b) at 5.5 GHz.

### 3.2. Results and Discussions of the Integrated Antenna in a Free-Space Environment

The objective of this work is to develop a gain-enhanced dual-band antenna to support WLAN/WBAN applications. Therefore, a $3 \times 3$ AMC array was selected as the back reflector and integrated with the antenna. Its overall physical dimensions were $49\,\text{mm} \times 49\,\text{mm}$ ($0.4\lambda_0 \times 0.4\lambda_0$). The AMC array and CPW-antenna were fabricated on an FR4 substrate with a thickness of 1 mm and 0.2 mm, respectively. The top view of the integrated antenna is shown in Figure 8(a). Figure 8(b) illustrates the antenna system supported by an AMC array, where the multi-band antenna is positioned above the center of the suggested AMC plane to serve as a reflector, with a distance denoted as '$h$', which indicates the separation between the AMC plane and the radiating patch. A foam piece with a permittivity nearly identical to air is placed between the antenna and AMC plane to bridge the gap between them. Figure 9(b) presents the return loss for the proposed AMC-backed antenna with various '$h$' values. It is evident that the impedance bandwidths of the AMC-backed antenna are significantly influenced by the value of '$h$'. In order to balance the AMC-backed antenna sys-

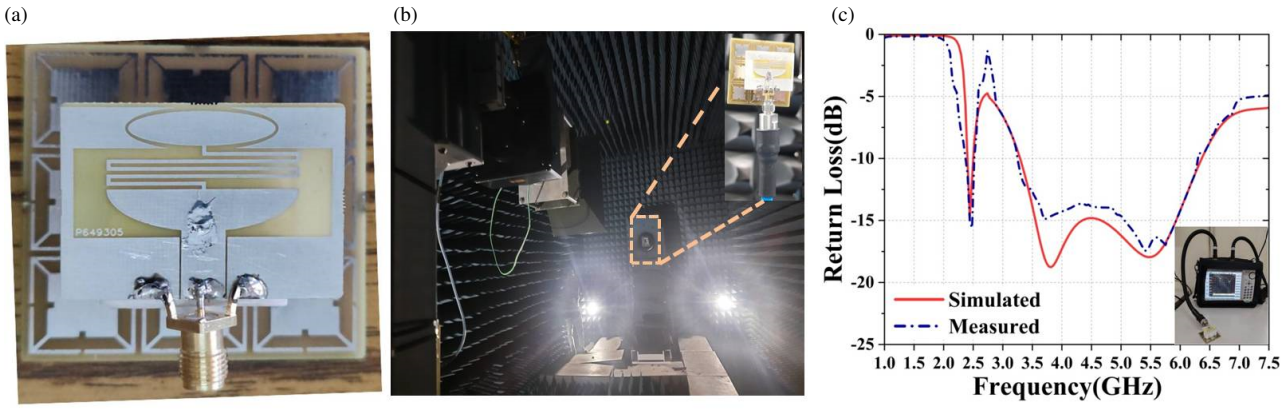


**FIGURE 11**. (a) Layout of fabricated antenna. (b) Antenna radiation pattern measurement setup. (c) Simulated and measured return loss comparison of antenna.

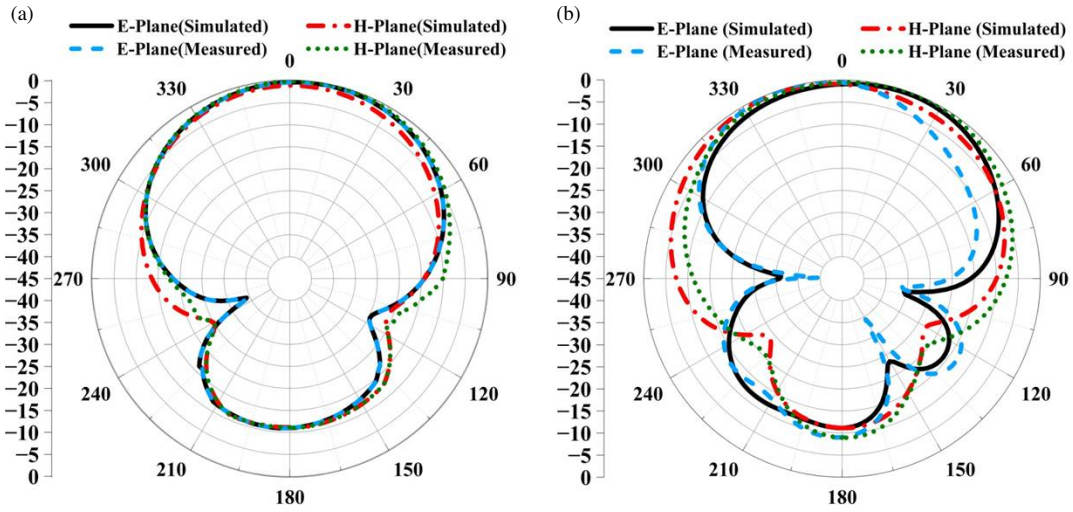


**FIGURE 12**. Comparison of measured and simulated radiation patterns (a) at 2.45 GHz, (b) at 5.5 GHz.

tem's performance with its multiband capability for the desired frequencies, the optimized value of '$h$' is 22 mm. With this configuration, the integrated antenna exhibits an impedance bandwidth of 8.20% between 2.3 and 2.5 GHz, a bandwidth of 65.90% between 3.2 and 6.35 GHz, and resonates at the required frequencies of 2.45 GHz and 5.5 GHz, as shown in Figure 9(b).

The simulated return loss of the proposed integrated antenna and the antenna alone in free space is illustrated in Figure 9(a). It has been noted that the upper frequency spectrum of a combined structure experiences a slight reduction in bandwidth compared to an isolated antenna. This decline is attributed to mutual coupling effects affecting impedance matching and radiation characteristics, along with inherent losses associated with the AMC array integrating with the antenna [14].

It is well known that gain improvement has been considered an essential feature of any antenna supported by an AMC array. As shown in Figure 9(c), it is evident that using the AMC array results in a gain improvement of $-2.5$ dBi to 7.56 dBi at 2.45 GHz and 3.5 dBi to 5.2 dBi at 5.5 GHz. When the AMC array is utilized to minimize the back radiation, the antenna radiation pattern has been transformed from omnidirectional to unidirectional. This transition is clearly demonstrated in the normalized polar plots of the radiation pattern for both the $E$-plane and $H$-plane at 2.45 GHz and 5.5 GHz, as depicted in Figures 10(a) and (b), respectively. The integrated antenna in both cases has shown a unidirectional radiation pattern (red line), which significantly lowered the front-to-back ratio (FBR). On the other hand, the antenna exhibits an omnidirectional radiation pattern (black dotted line) in the absence of the AMC array.

#### 3.2.1. Observations on Simulated and Measured Results

To confirm the effectiveness of the suggested antenna, a CPW antenna including an AMC surface was fabricated and presented in Figure 11(a).

The prototype was measured for return loss using the Anritsu S820E Site Master Handheld Cable & Antenna Analyzer. The obtained results were then compared to the simulated data. The comparison of simulated and measured return losses is shown in Figure 11(c). According to the measured results, the integrated antenna operated at 2.3–2.5 GHz and 3.2–6.35 GHz for $S_{11}$ <

**TABLE 2**. Proposed wearable antenna in comparison to other dual-band antennas.

| References | Size ($mm^2$) | Frequency of operation (GHz) | Antenna with/without reflector | Gain (dBi) |
|---|---|---|---|---|
| **Proposed work** | $49 \times 49$ | **2.45** | **AMC Array** | **7.56** |
| | | **5.50** | | **5.50** |
| **[7]** | $200 \times 200$ | **2.45** | **AMC Array** | **2.50** |
| | | **5.20** | | **3.50** |
| **[10]** | $44.4 \times 44.4$ | **2.45** | **AMC Array** | **4.88** |
| | | **5.80** | | **4.73** |
| **[21]** | $50 \times 50$ | **2.40** | **AMC Array** | **0.12** |
| **[22]** | $44.1 \times 44.1$ | **2.45** | **AMC Array** | $-0.67$ |
| | | **5.50** | | **7.40** |
| **[23]** | $48 \times 48$ | **2.50** | **AMC Array** | **6.50** |
| **[24]** | $67.2 \times 67.2$ | **2.45** | **AMC Array** | **5.23** |

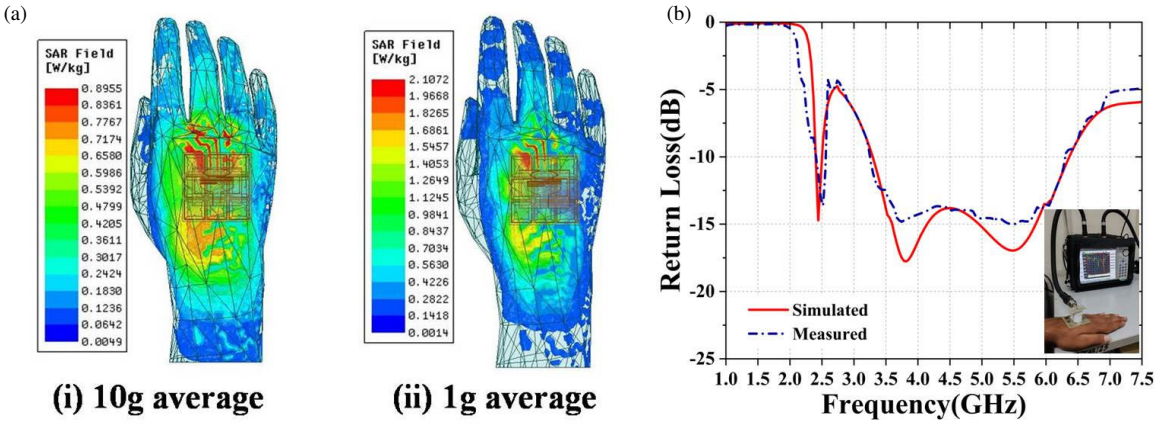


**FIGURE 13**. Assessment of antenna SAR using a human hand model. (a) Three-dimensional SAR distribution of antenna at 5.5 GHz on hand position. (b) Simulated and measured return loss of the integrated antenna when placed over the hand model.

$-10$ dB. The two were found to be strongly in agreement with the simulated outcomes, indicating the validity of the simulated data.

To validate the accuracy of the simulations, the radiation pattern of the antenna was assessed within an anechoic chamber, as shown in Figure 11(b). In Figure 12, the comparison between the simulated and measured normalized radiation patterns in the $E$-plane and $H$-plane at 2.45 and 5.5 GHz are depicted, showing good agreement between the simulated and measured results. The spatial radiation patterns in the $E$-plane and $H$-plane exhibit slight asymmetry, which is attributed to the current imbalance on the meander-line connecting the elliptical patch and semi-elliptical patch [20]. In addition, any disparities noted could be attributed to factors such as heightened dielectric loss, imperfect soldering, and variations in measurement tolerances [11]. Furthermore, the experimental results showed that the suggested antenna has maximum peak gains of 7.56 dBi and 5.5 dBi at 2.45 GHz and 5.5 GHz, respectively, and $\theta = 0°$ is the major lobe direction where the gain values are observed. Table 2 presents a comparison between the newly proposed antenna and the current state-of-the-art dual-band wearable antenna found in existing literature.

### 3.3. Observations on the Impact of Human Body Loading on Integrated Antenna Performance

The secondary main purpose of the AMC reflector backing is to provide protection for the antenna from the adverse impacts of nearby highly dielectric and lossy human bodies, thus maintaining antenna performance. The integrated antenna reflection coefficient was evaluated against human hand model, as shown in Figure 13(a). The antenna whose performance has to be tested is positioned 1 mm from the model. Figure 13(b) illustrates the simulated and measured return losses of the combined layout when it is placed over the hand model. It has been observed that the return loss of the antenna is not affected by human-hand model loading.

To ensure safety standards for wearable devices, the antenna needs to adhere to Specific Absorption Rate (SAR) guidelines. According to the IEEE standard [25, 26], SAR regulations mandate that the average SAR over 1 gram of tissue must remain under 1.6 W/kg, while over 10 grams of tissue it should be below 2 W/kg. This study will primarily concentrate on SAR measurements concerning 10 gram of tissue to remain simple.

**TABLE 3**. Comparison between the simulated maximum SAR of the antenna in isolation and the integrated antenna loaded on the human hand model.

| Antenna Configuration | 1 g/10 g | Frequency (GHz) | Max. SAR (W/kg) |
|---|---|---|---|
| **Antenna without AMC array (1 mm separation from hand model)** | 1 g | 2.45 | 18.8716 |
| | | 5.50 | 20.6723 |
| | 10 g | 2.45 | 12.7710 |
| | | 5.50 | 9.6345 |
| **Antenna with AMC array (1 mm separation from hand model)** | 1 g | 2.45 | 1.8362 |
| | | 5.50 | 2.1072 |
| | 10 g | 2.45 | 1.2032 |
| | | 5.50 | 0.8955 |

Figure 13(a) illustrates the SAR distribution of the antenna at 5.5 GHz in the on-hand position.

Furthermore, the SAR has been evaluated and compared using an input power of 1 W, as shown in Table 3. It has been noticed that the incorporation of the AMC array behind the desired antenna resulted in reductions of almost 90%. Here, in order to satisfy the SAR requirements, the maximum allowable input power can be varied based on the targeted applications.

## 4. CONCLUSION

This paper demonstrates an integrated antenna consisting of a CPW-fed wearable antenna combined with a $3 \times 3$ AMC array for WBAN/WLAN applications. The antenna under consideration operates at 2.45 GHz and 5.5 GHz, with maximum gains of 7.56 dBi and 5.5 dBi, respectively, while maintaining a gain at least 5.2 dBi across its operational bandwidth. Furthermore, it has been shown that the inclusion of the AMC array results in a significant gain enhancement and a 90% reduction in SAR at both resonant frequencies compared to an isolated CPW-fed antenna. The fabricated CPW-antenna prototype, along with the AMC array, was tested on various human body models. The experimental results have been consistent with those obtained from simulation. The suggested antenna offers benefits such as broad bandwidth, minimal back radiation, and enhanced gain. The results suggest that the integrated antenna presented in this study has the potential for the use in wearable medical applications.

## REFERENCES


[1] Hall, P. S. and Y. Hao, *Antennas and Propagation for Body-centric Wireless Communications*, Artech House, Norwood, MA, USA, 2012.

[2] Fang, G., E. Dutkiewicz, M. A. Huq, R. Vesilo, and Y. Yang, "Medical body area networks: Opportunities, challenges and practices," in *2011 11th International Symposium on Communications & Information Technologies (ISCIT)*, 562–567, Hangzhou, China, 2011.

[3] Musa, U., S. M. Shah, H. A. Majid, I. A. Mahadi, M. K. A. Rahim, M. S. Yahya, and Z. Z. Abidin, "Design and analysis of a compact dual-band wearable antenna for WBAN applications," *IEEE Access*, Vol. 11, 30 996–31 009, 2023.

[4] Liu, Z.-G. and Y.-X. Guo, "Compact low-profile dual band metamaterial antenna for body centric communications," *IEEE Antennas and Wireless Propagation Letters*, Vol. 14, 863–866, 2014.

[5] Tak, J., S. Woo, J. Kwon, and J. Choi, "Dual-band dual-mode patch antenna for on-/off-body WBAN communications," *IEEE Antennas and Wireless Propagation Letters*, Vol. 15, 348–351, 2015.

[6] Sharma, S. K. and R. K. Chaudhary, "A compact zeroth-order resonating wideband antenna with dual-band characteristics," *IEEE Antennas and Wireless Propagation Letters*, Vol. 14, 1670–1672, 2015.

[7] Wu, X., X. Wen, J. Yang, S. Yang, and J. Xu, "Metamaterial structure based dual-band antenna for WLAN," *IEEE Photonics Journal*, Vol. 14, No. 2, 1–5, Apr. 2022.

[8] Zhang, H., X. Chen, M. Li, F. Yang, and S. Xu, "A compact dual-band folded-cavity antenna for microwave biomedical imaging applications," in *2019 IEEE International Conference on Computational Electromagnetics (ICCEM)*, 1–3, Shanghai, China, Mar. 2019.

[9] Yan, S., P. J. Soh, and G. A. E. Vandenbosch, "Low-profile dual-band textile antenna with artificial magnetic conductor plane," *IEEE Transactions on Antennas and Propagation*, Vol. 62, No. 12, 6487–6490, Dec. 2014.

[10] Ahmad, S., K. N. Paracha, Y. A. Sheikh, A. Ghaffar, A. D. Butt, M. Alibakhshikenari, P. J. Soh, S. Khan, and F. Falcone, "A metasurface-based single-layered compact amc-backed dual-band antenna for off-body iot devices," *IEEE Access*, Vol. 9, 159 598–159 615, 2021.

[11] Jiang, Z., Z. Wang, L. Nie, X. Zhao, and S. Huang, "A low-profile ultrawideband slotted dipole antenna based on artificial magnetic conductor," *IEEE Antennas and Wireless Propagation Letters*, Vol. 21, No. 4, 671–675, Apr. 2022.

[12] Jagtap, S., A. Chaudhari, N. Chaskar, S. Kharche, and R. K. Gupta, "A wideband microstrip array design using RIS and PRS layers," *IEEE Antennas and Wireless Propagation Letters*, Vol. 17, No. 3, 509–512, Mar. 2018.

[13] Bahl, I. J., *Lumped Elements for RF and Microwave Circuits*, Artech House, 2003.

[14] Caloz, C. and T. Itoh, *Electromagnetic Metamaterials: Transmission Line Theory and Microwave Applications*, John Wiley & Sons, 2005.

[15] Jang, T., J. Choi, and S. Lim, "Compact coplanar waveguide (CPW)-fed zeroth-order resonant antennas with extended bandwidth and high efficiency on vialess single layer," *IEEE Transactions on Antennas and Propagation*, Vol. 59, No. 2, 363–372,

Feb. 2011.

[16] Chu, L. J., "Physical limitations of omnidirectional antennas," *Journal of Applied Physics*, Vol. 19, No. 12, 1064–1076, 1948.

[17] McLean, J. S., "A re-examination of the fundamental limits on the radiation Q of electrically small antennas," *IEEE Transactions on Antennas and Propagation*, Vol. 44, No. 5, 672–676, May 1996.

[18] Foroozesh, A. and L. Shafai, "Investigation into the application of artificial magnetic conductors to bandwidth broadening, gain enhancement and beam shaping of low profile and conventional monopole antennas," *IEEE Transactions on Antennas and Propagation*, Vol. 59, No. 1, 4–20, Jan. 2011.

[19] Kern, D. J., D. H. Werner, A. Monorchio, L. Lanuzza, and M. J. Wilhelm, "The design synthesis of multiband artificial magnetic conductors using high impedance frequency selective surfaces," *IEEE Transactions on Antennas and Propagation*, Vol. 53, No. 1, 8–17, Jan. 2005.

[20] Gupta, A. and R. K. Chaudhary, "A compact dual band short ended metamaterial antenna with extended bandwidth," *International Journal of RF and Microwave Computer-Aided Engineering*, Vol. 26, No. 5, 435–441, Mar. 2016.

[21] Agarwal, K., Y.-X. Guo, and B. Salam, "Wearable AMC backed near-endfire antenna for on-body communications on latex substrate," *IEEE Transactions on Components, Packaging and Manufacturing Technology*, Vol. 6, No. 3, 346–358, Mar. 2016.

[22] Zhang, K., P. J. Soh, and S. Yan, "Design of a compact dual-band textile antenna based on metasurface," *IEEE Transactions on Biomedical Circuits and Systems*, Vol. 16, No. 2, 211–221, Apr. 2022.

[23] Kaur, K. and A. Kaur, "Metamaterial based AMC backed archimedean spiral antenna for in-vitro microwave hyperthermia of skin cancer," *Electromagnetic Biology and Medicine*, Vol. 42, No. 4, 163–181, Dec. 2023.

[24] Ali, U., S. Ullah, A. Basir, B. Kamal, L. Matekovits, and H. Yoo, "Design and SAR analysis of AMC-based fabric antenna for body-centric communication," *IEEE Access*, Vol. 11, 73 894–73 911, Jul. 2023.

[25] "IEEE standard for safety levels with respect to human exposure to radio frequency electromagnetic fields, 3 kHz to 300 GHz," IEEE Std C95.1-1999, 1999.

[26] "IEEE standard for safety levels with respect to human exposure to radio frequency electromagnetic fields, 3 kHz to 300 GHz," (Revision of IEEE Std C95.1-1991), 2006.